5
Calculation of Semiconductor Band Structures and Defects by the Screened Exchange Density Functional

S. J. Clark and John Robertson

5.1
Introduction

The local density approximation (LDA) is an efficient method to solve the eigenvalue equation of the many-body electronic Hamiltonian. The simplicity of LDA is to represent the exchange–correlation energy E_{xc} as a functional of the electron density, not the wave function. However, DFT under estimates the band gap of semiconductors and insulators [1]. Typically, the error is 30%, but the error can be 70% in cases like ZnO or even negative gaps in cases like InAs. This causes severe problems in the treatment of point defects and for heterojunction interfaces.

Various methods can be used to correct the band gap problem of the LDA and generalized gradient approximations (GGA). The first method is the scissors operator [2], in which the conduction band is just rigidly shifted upwards to fit the experimental band gap. This is not suitable for defect calculations.

Another correction method is the self-interaction correction (SIC) method of Perdew and Zunger [3] but this is still difficult to implement [4]. The GW method is widely used to provide accurate band structures [5–10], but it is very expensive, is usually too costly for defect calculations using supercells, and it cannot be used variationally to find geometries.

The LDA + U method has been used to correct band structures in open shell systems, where an on-site repulsion energy U is used to open up a gap between spin-up and spin down electrons [11, 12]. However, this method is only valid for open-shell systems. It is not valid for the standard closed shell semiconductors and insulators. For semiconductors with shallow core states such as ZnO, the LDA + U method can be used to partly correct the band gap, by forcing the Zn 3d states down, and thus reducing their repulsion from below on the valence band maximum state [13]. Any use of LDA + U to fit the band gap of closed shell systems will require an unphysical value of U.

The local exchange and correlation functionals of LDA and GGA lead to a spurious electronic self-interaction. The HF method uses a non-local exchange, so that it can be

Advanced Calculations for Defects in Materials: Electronic Structure Methods, First Edition.
Edited by Audrius Alkauskas, Peter Deák, Jörg Neugebauer, Alfredo Pasquarello, and Chris G. Van de Walle.

self-interaction free, but HF lacks electronic correlation, and its exchange is unrealistically long-ranged due to an absence of screening.

In the late 1990s, it was realized that mixing in a fraction of Hartree–Fock exchange into the LDA exchange–correlation energy could be used to correct the band gap error and make the eigenvalues of the Kohn–Sham equations equal to the quasi-particle energies. Becke [14] gave arguments based on an adiabatic linkage of the HF and LDA limits that 25% is an appropriate amount of HF exchange to mix into the local exchange–correlation functional. This gave rise to the so-called hybrid functionals, such as B3LYP [14] and the PBEh [15] hybrid, formerly known as PBE0, in which 25% of Fock exchange is substituted into the LDA of E_{xc}. Muscat *et al.* [16] found that B3LYP gave good values for the band gaps of various semiconductors. The PBEh also mixes in 25% of HF exchange, and gives reasonable band gaps [17].

The HF exchange is unrealistically long-range due to an absence of screening, and is divergent for a plane wave basis. This led to the development of the screened hybrid functionals of Heyd–Scuseria–Erzenhof (HSE) [18–21] by separating the non-local HF exchange into long and short-range parts, and replacing a fraction (again, $\alpha = 0.25$) of the short-range parts of the LDA exchange with HF exchange. This is based on the notion that the exchange and correlation terms cancel at long range. The retention of only short-range HF exchange allows faster calculations. HSE is a variational functional that can be used for energy minimization. HSE was implemented for a local orbital basis and it has been tested on various molecules and solids [20, 21], and later for a plane wave basis with projector augmented waves [22].

Earlier and in a similar way, Bylander and Kleinman [23] proposed a similar separation of long and short ranged parts of the screened exchange (SX) [5]. They represented the exchange interaction by a Thomas–Fermi screened Coulomb potential, and use the LDA correlation. It has similar attributes to HSE. Seidel *et al.* [24] realized that SX was a variational functional, and so it was suitable for geometry optimization. Previously, Freeman and coworkers [25, 26] have used SX extensively to calculate the band structures of semiconductors, some oxides and their optical properties. It was not used for energy minimization, which is done here.

5.2
Screened Exchange Functional

The non-local XC potential of SX is similar in form to the HF potential, but it also incorporates the effects of correlation by screening the long-range interactions of exchange [23]. The non-local contribution to the total energy of the system is

$$E_{\mathrm{nl}}^{\mathrm{SX}} = -\frac{1}{2}\sum_{ij,kq}\int\int \frac{\psi_{ik}^{*}(r)\psi_{ik}(r')\exp\left(-k_{\mathrm{s}}|r-r'|\right)\psi_{jq}^{*}(r')\psi_{jq}(r)}{|r-r'|}\,\mathrm{d}r\,\mathrm{d}r', \tag{5.1}$$

where i and j label electronic bands, k and q the k-points and k_s is a Thomas–Fermi screening length.

In order to maintain the exact expression for the homogeneous electron gas (HEG), a local (loc) contribution is also required, so that the total exchange–correlation energy in the screened-exchange method is

$$E^{SX} = E^{SX}_{nl} + E^{SX}_{loc},$$

where E^{SX}_{loc} is this additional contribution which is parameterized using Perdew's expression for the LDA [3]. Thus the local contribution to the exchange and correlation energy density is

$$\varepsilon^{SX}_{loc}(\varrho) = \varepsilon^{HEG}_{loc}(\varrho) - \varepsilon^{HEG}_{nl}(\varrho), \tag{5.2}$$

where the local $\varepsilon^{HEG}_{loc}(\varrho)$ is the same as the LDA (HEG). The second term is obtained by applying the non-local functional to the HEG, which is given by

$$\varepsilon^{HEG}_{nl}(\varrho) = V^{HEG}_{X}(\varrho) F(\varrho), \tag{5.3}$$

where V_x is the pure HF exchange of the HEG, $F(\varrho)$ is a screening function given in Eq. (5.3) in Bylander and Kleinman [23]. Thus the total exchange–correlation energy within the screened-exchange formalism is

$$E^{SX} = E^{SX}_{nl} + E^{HEG}_{loc} - \int V^{HEG}_{X}(\varrho) F(\varrho) \varrho(r)\, dr. \tag{5.4}$$

This is analogous to the HSE term where the first term represents the '$\alpha = 0.25$' of HF, the second term is the long-ranged exchange and the final term is similar to the short-ranged-screened local PBE exchange of HSE. An important factor is that SX reproduces the correct asymptotic limits of XC in both the free electron gas and the HF limit.

The SX method has been implemented in the CASTEP code [27], a plane wave pseudopotential code. It uses norm-conserving pseudopotentials. In many cases, more transferable pseudopotential was generated using the Opium code [28]. The Thomas Fermi (TF) screening parameter is found from the valence electron density by $k_s = 2(k_F/\pi)^{1/2}$ where k_F is the Fermi wavenumber. There are two options, either k_s is set to the average valence electron density of the system, or it is given by a fixed value, such as the natural density of the HEG. In cases of shallow d core states, these can be included in the valence states, but those core electrons are *not* counted in the TF parameter. Non-local stresses are evaluated by the scheme of Gibson *et al.* [29], which now allows the efficient geometry optimization of the unit cell.

SX is efficient, so that it can be used to carry out the full geometry relaxations in realistic-sized defect supercells, and not just as a post-processing of geometries found by LDA or GGA. It is expected to have similar efficiency to HSE, but this depends on the implementation and the screening lengths used.

5.3
Bulk Band Structures and Defects

Table 5.1 compares the calculated SX band gaps with those calculated by GGA and the experimental values. It can be seen that there is a significant improvement. These are also shown in Figure 5.1. Notable cases are for Si the band gap improves from 0.69 to

Table 5.1 Comparison of the calculated GGA and SX bands gap to the experimental values are given. Also presented are the calculated GGA and SX lattice constants, which are compared to the experimental values.

compound	PBE band gap (eV)	SX band gap (eV)	exp band gap (eV)	GGA lattice constant (Å)	SX lattice constant (Å)	exp lattice constant (Å)
diamond	4.27	5.38	5.5	3.537	3.501	3.567
Si	0.69	1.07	1.12	5.401	5.397	5.431
Ge	0.59	0.69	0.7	5.478	5.414	5.657
c-SiC	1.47	2.25	2.42	4.320	4.262	4.348
AlP	1.66	2.21	2.45	5.438	5.386	5.451
AlAs	1.58	2.30	2.24	5.640	5.581	5.62
AlSb	1.57	1.83	1.70	6.063	6.021	6.13
GaP	1.70	1.85	1.9	5.502	5.374	5.45
GaAs	0.87	1.47	1.45	5.707	5.570	5.66
GaSb	1.00	1.13	0.82	6.066	5.905	6.09
ZnO(zb)	0.89	3.43	3.44	4.583	4.586	4.51
ZnO (wz)	0.8	3.41	3.44	3.268/5.299	3.27/5.25	3.25/5.21
ZnS	2.15	3.74	3.80	5.606	5.421	5.41
ZnSe	1.68	2.71	2.82	5.875	5.569	5.67
ZnTe	1.81	2.34	2.39	6.280	6.025	6.089
CdS	1.59	2.38	2.42	5.983	5.865	5.818
CdSe	1.33	1.88	1.84	6.245	6.113	6.05
CdTe	1.67	1.71	1.60	6.652	6.486	6.48
MgS (rs)	2.77	3.70	3.7	5.210	5.167	5.20
MgS (zb)	3.37	4.84	4.8	5.659	5.599	5.66
MgSe (zb)	2.95	3.91	4.0	5.949	5.893	5.91
CdO	−0.60	0.98	0.9	4.708	4.670	4.69
MgO	3.60	7.72	7.8	4.223	4.126	4.21
LiF	9.24	13.27	13.7	4.093	4.032	4.017
SiO_2	6.05	8.74	9	4.909/5.402	4.855/5.371	5.01/5.47
α-Al_2O_3	6.25	8.64	8.8	4.76/13.00	4.70/12.97	4.76/12.99
SnO_2	0.93	3.66	3.6	4.738/3.149	4.692/3.136	4.737/3.186
In_2O_3	0.90	3.03	2.9	10.118	10.016	10.12
Cu_2O	1.04	2.11	2.12	4.359	4.315	4.27
TiO_2	1.86	3.1	3.2	4.691/2.994	4.608/2.920	4.59/2.96
c-HfO_2	3.74	5.60	5.8	5.161	5.037	5.11
c-ZrO_2	3.43	5.76	5.7	5.131	5.022	5.07
SrTiO3	1.93	3.28	3.2	3.971	3.874	3.905
$PbTiO_3$	1.71	3.43	3.4	3.983	3.904	3.96

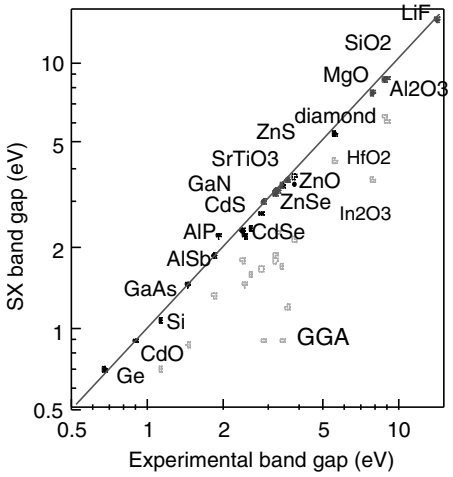

Figure 5.1 (online colour at: www.pss-b.com) GGA and SX band gaps, compared to experiment values. Closed Circles refer to the SX band gap, open circles refer to the GGA band gap.

1.07 eV compared to 1.19 eV experimentally. For GaAs, the band gap increases from 0.87 eV in GGA to 1.47 eV in SX. For insulators, SiO_2, the gap improves from 6.0 eV in GGA to 8.74 eV in SX, very close to the 9.0 eV experimental value. For wide gap insulators such as LiF, the gap is 13.27 eV in SX, 9.24eV in PBE, compared to 13.7 eV experimentally. It has been used before on HfO_2 and the multiferroic $BiFeO_3$ [30–32].

The improvement is most significant for the transparent conducting oxides such as ZnO, In_2O_3 and SnO_2. These band structures are characterized by a single, broad conduction band minimum at Γ. The minimum gap of SnO_2 is 0.9 eV in GGA, and this becomes 3.66 eV in SX, compared to 3.6 eV found experimentally. The reason is that direct gap at Γ is unrepresentative of the averaged gap. The average gap opens up by the typical 20%, but this translates into a very large fractional change at Γ.

5.3.1 Band Structure of ZnO

ZnO is an important semiconductor, which is widely used as a phosphor, for transparent electrodes in solar cells, and for ultraviolet light emission, spintronics, nanowires and for its high electron mobility [33–39]. It can be easily doped n-type but it is difficult to dope p-type [35]. This has been attributed to the nature of its intrinsic defects which cause a self-compensation of free carriers [40] and also to that common acceptors are deep [41]. It is therefore important to understand the energetics of its intrinsic defects.

There have been numerous first-principles studies of the bulk electronic structure of ZnO [13, 42–48] and its defect energies [49–63].The LDA + U method has been used to improve the GGA band structure, by shifting the Zn 3d band downwards [13]. The SIC method has been used to find the band structure of ZnO [44]. Various

types of GW methods have been used for ZnO [45–47]. The HSE hybrid has been used [47, 48, 52, 56, 61].

Defect calculations generally find that the O vacancy is the defect with lowest formation energy but it is deep, while the Zn interstitial is shallow but has higher formation energy. Nevertheless, there is a lack of consistency between the various results. This arise partly because of the band gap error of LDA and also sometimes because charge state corrections were not correctly included.

Patterson [54] used the B3LYP functional and localized orbitals to calculate the defect eigenvalues, but he did not calculate the defect formation energies from the total energies. Oba *et al.* [52] used the HSE functional to provide a complete set of defect formation energies, and tested the corrections for supercell size. Superficially, this is a well-defined calculation. However, it was necessary to increase the HF mixing parameter a from $a = 0.25$ to 0.375 in order to empirically fit the experimental gap. Agoston *et al.* [56] produced a valuable comparison of GGA and HSE results for O vacancies for all three conducting oxides.

Recently, we applied the SX method to the intrinsic defects of ZnO [61]. For our SX calculations, k_s is determined from the valence electron density, and for those elements like Zn with shallow filled d states, it is for s, p electrons only. The $k_{TF} = 2.27\,A^{-1}$ for ZnO. A plane-wave cut-off energy of 800 eV is used, which converges total energy differences to better that 1 meV/atom. Integrations over the Brillouin zone are performed using the k-point sampling method of Monkhorst and Pack with a grid that converges the energies of the bulk unit cell to a similar accuracy. Geometry optimizations are performed self-consistently using a minimization scheme and the Hellmann–Feynman forces, and are converged when forces are below 0.04 eV/Å.

Table 5.2 shows the converged lattice parameters of ZnO, which are within 0.5% of experiment, whereas GGA (PBE) values are 1% too large. The free energy of ZnO per formula unit is found to be only 0.3 eV less than experiment, a 60% improvement over the PBE result.

Figure 5.2 shows the calculated band structure of bulk ZnO in the wurtzite and zincblende structure. The minimum gap is calculated to be 3.41 eV, and is very close to the 3.44 eV found experimentally [35]. Our value is much closer to experiment than HSE with the normal a parameter (2.87 eV) [48], or even with the expensive GW [45] which gets 2.7 eV.

Table 5.2 Bulk properties of wurzite ZnO, calculated compared to experiment.

	GGA	SX	exp
a (Å)	3.286	3.267	3.2495
c (Å)	5.299	5.245	5.2069
free energy (eV)	−2.82	−3.31	−3.63
direct gap (eV)	0.9	3.41	3.44
Zn 3d (eV)	−4.8	−7.0	−7.3

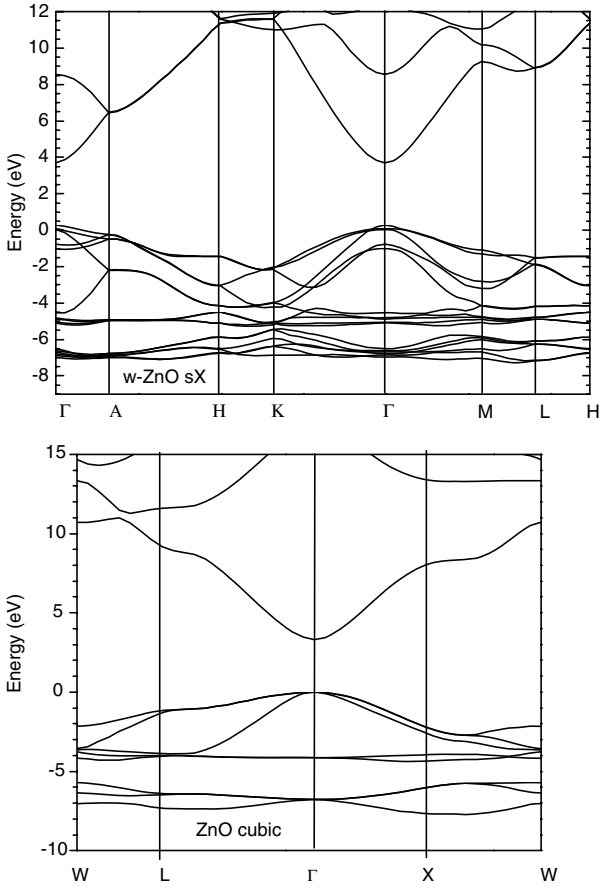

Figure 5.2 The band structure of ZnO in the wurtzite and zincblende structures evaluated using the SX functional.

Part of the LDA band gap error in ZnO arises from the Zn 3d (t_{2g}) levels lying too high, and their upwards repulsion of the Γ_{15} valence band maximum states. In SX, the Zn 3d states now lie at −7.0 below the VB maximum, very close to where they are found experimentally by angle-resolved photoemission [64, 65].

5.3.2
Defects of ZnO

The defect calculations are carried out using a 120 atom supercell, whose size is fixed at that of the defect-free cell, and the defect created. The internal geometry is relaxed within SX, using a single special *k*-point of (1/4, 1/4, 1/3) for Brillouin zone integrations, which converges the quantities faster than the Γ point with respect to supercell size [66].

The total energy (E_q) is calculated for the defect cell of charge q, for the perfect cell (E_H) of charge q, and for a perfect cell of charge 0. This allows us to calculate the defect formation energy, H_q, as a function of the relative Fermi energy (ΔE_F) from the valence band edge E_V and the relative chemical potential ($\Delta\mu$) of element α [60],

$$H_q(E_F, \mu) = [E_q - E_H] + q(E_V + \Delta E_F) + \sum_\alpha n_\alpha(\mu_\alpha^0 + \Delta\mu_\alpha),$$

where $q(E_V + \Delta E_F)$ is the change in energy when charge q is added to the system at the Fermi level and n_α is the number of atoms of species α. Essentially, this is the shift in the average electrostatic potential due to the charge of the system with respect to the uncharged system. The corrections for the background charge, band filling, etc., are included as described in Ref. [58]. The oxygen chemical potential (μ^0) is referred to that of the O_2 molecule, taken as zero, which is the O-rich limit. The O-poor limit corresponds to the Zn/ZnO equilibrium and is $\mu(O) = -3.31$ eV (the heat of formation of ZnO).

Figure 5.3a and b shows the calculated formation energies of the four intrinsic defects of ZnO in the O-rich and O-poor limits. We see that the O vacancy (V_O) has the lowest formation energy over a wide range of E_F, lower than the Zn interstitial. V_O is a deep defect and it has a transition state between its neutral and doubly positive states $E(0/2+)$ at 2.20 eV. The $+1$ state is never stable, so the O vacancy has a negative effective correlation energy (U), as found by others. We find $U = -2.0$ eV, the energy difference between the metastable $0/+$ and $+/2+$ transitions in Figure 5.4. The negative U arises because of the strong lattice relaxation with changing charge state, with the Zn-vacancy distance changing from 1.84 Å for V^0, to 2.16 Å for V^+ to 2.46 Å for V^{2+}, compared to a bulk Zn–O distance of 1.95 A.

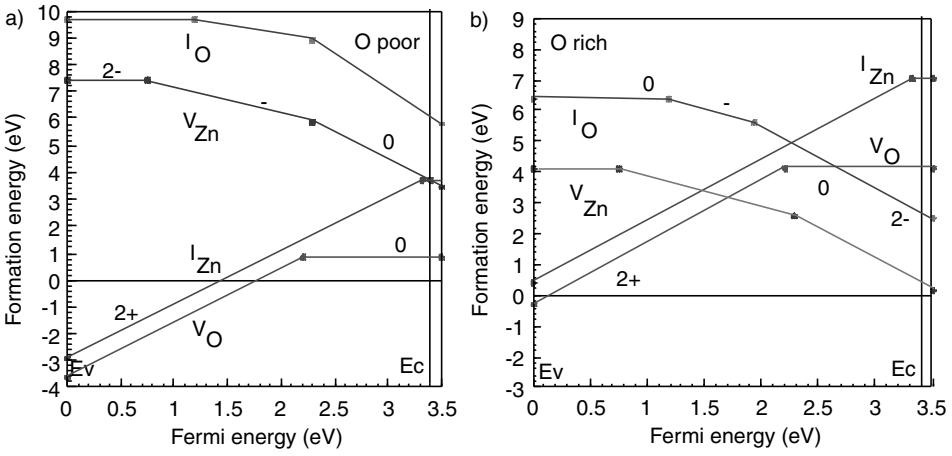

Figure 5.3 (online colour at: www.pss-b.com) The formation energies of native defects in ZnO evaluated using the SX functional under (a) oxygen poor and (b) oxygen rich conditions. The gradients of the lines give the charge state of the defect.

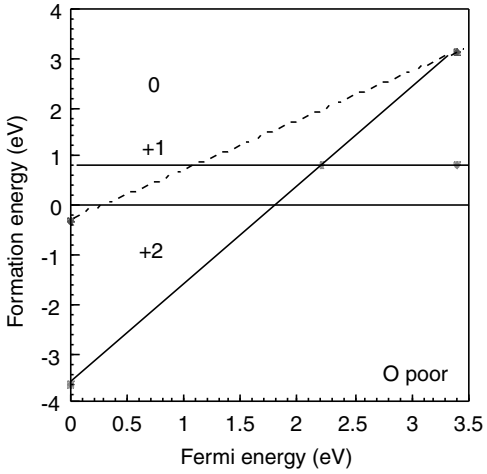

Figure 5.4 (online colour at: www.pss-b.com) The formation energy of the neutral, +1 and +2 charge states of the oxygen vacancy in ZnO under oxygen poor conditions.

These relaxations are seen in Figure 5.5a–c. Note that the relaxed structures found by SX are similar to those found by GGA, so in fact in this case, we could have used SX post-processing on GGA structures to find the defect formation energies.

We find that the Zn interstitial I_{Zn} is a shallow defect, with a slightly higher formation energy than V_O. Its transition state $(0/2+)$ lies at 3.32 eV, essentially at the conduction band edge, consistent with experiment [37], and it has a $U = 0$ eV. However, its neutral state has a large formation energy in O^- poor conditions.

The other two intrinsic defects I_O and V_{Zn} are more stable in O-rich conditions (compared to V_O and I_{Zn}), and have higher formation energies. They are both deep defects, and show two charge states in the gap, corresponding to positive U behaviour. The I_O forms the usual dumb-bell structure of O interstitials in its 0 and − charge states, while the I_{Zn} sits in the octahedral site as seen by others [50].

Figure 5.6 compares our formation energies of the O vacancy to those calculated by others. The calculated formation energy of V^0 of +0.85 eV in SX is similar to that found by Lany and Zunger [59], slightly less than the 1.0 eV found by Oba *et al.* [52], and similar to that found by Agoston *et al.* [56]. However, it is much less than the formation energy given by Janotti and van de Walle [50]. The +0.85 eV formation energy would correspond to a frozen-in vacancy concentration of 10^{19} cm^{-3} at 700 °C, which is consistent with the concentration found experimentally [67, 68]. However, being deep, it is not a source of free electrons. The large formation energy of neutral Zn interstitial means that this cannot be the source of free electrons in ZnO, as its concentration would be too low [69]. This means that in the absence of hydrogen, the source of free electrons must be a donor complex.

Our $(0/2+)$ transition energy of 2.20 eV above the valence band top is the same as that found by Janotti and van de Walle [50, 51], by Oba *et al.* [52], and Agoston *et al.* [56], but higher than found by Lany in corrected GGA [59]. The metastable $(0/+)$

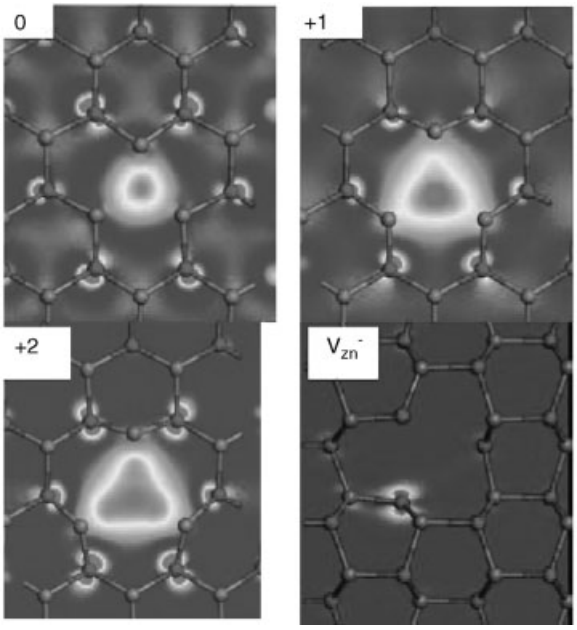

Figure 5.5 (online colour at: www.pss-b.com) In (a), (b) and (c), the electronic density of the defect state found in the band gap of ZnO is shown for the oxygen vacancy for the neutral, $+1$ and $+2$ charge states, respectively. In (d), the defect state of the Zn vacancy is shown and is found to be a p-like state located on only *one* of the adjacent oxygen atoms.

transition lies at 0.9 eV and this is consistent if the ODMR transition observed by Vlasenko and Watkins [70] is from valence band to the defect level. Thus, overall there is now a reasonable convergence in formation energies and transition energies between some of the calculations.

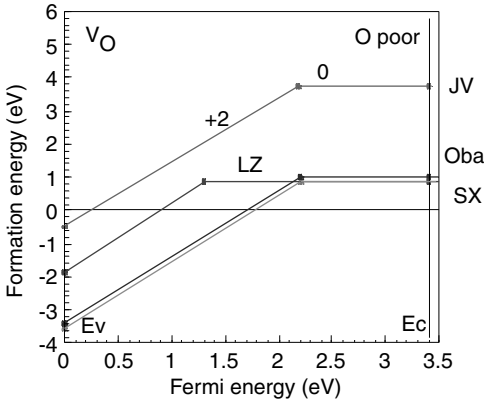

Figure 5.6 (online colour at: www.pss-b.com) The oxygen vacancy formation energy under oxygen poor conditions as a function of Fermi energy is shown for the present (SX) and other studies. Janotti and van de Walle (JV) [49], Lany and Zunger (LZ) [58], and Oba *et al*. [52].

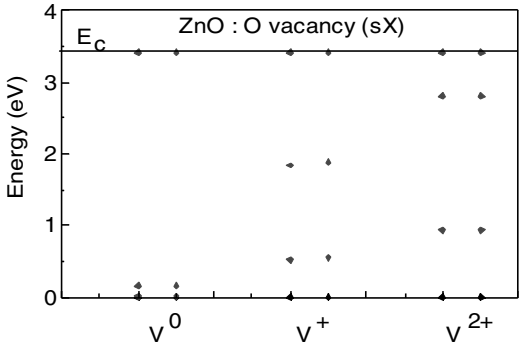

Figure 5.7 (online colour at: www.pss-b.com) The energy eigenvalues of the oxygen vacancy defect states lying in the band gap for SX.

It is interesting that for the oxygen vacancy, the SX and GGA relaxed atomic positions and wave functions are similar.

Figure 5.7 shows our calculated eigenvalues of the oxygen vacancy. We see that the eigenvalue of the neutral V_O lies at $+0.16$ eV above the VB top. In GGA, it lies in the lower gap. This is why V_O is able to display three charges even in GGA calculations despite the severe under-estimate of the gap. However, it does show that the calculated eigenvalues of V_O have little relationship to the transition energies in ZnO, due to the strong lattice relaxations. Hence the result of the B3LYP calculation of Patterson [54] is not particularly relevant, as it only gives transition energies.

Finally, the LDA is known to under-estimate the localization of hole states. For example, the trapped hole state of Al_{Si} in SiO_2 (smoky quartz) is well known to be trapped on a single oxygen, but LDA finds it localized on all four neighbouring oxygens [71]. There are other recent examples [71, 72]. Figure 5.5d shows the calculated SX charge density of the single trapped hole state of the Zn vacancy $V_{\overline{Zn}}$. We find it to be localized on one oxygen neighbour in SX, not four. In this case, the charge density in SX differs considerably from that of GGA. This is consistent with its spin resonance signature [73, 74]. Even LDA $+$ U cannot localize it on one oxygen [51]. On the other hand, the wave functions of the three states of V_O are localized over all four Zn neighbours, consistent with a simple symmetric vacancy (Figure 5.5a–c). The localization is driven by distortion. Thus, in this case, the SX and GGA geometries are different, we could not have found defect formation energies by post-processing GGA geometries in SX.

5.3.3
Band Structure of MgO

Figure 5.8 shows the SX band structure of the clasical metal oxide MgO. Its calculated band gap is 7.7 eV, which is close to the experimental value of 7.8 eV. The valence band is formed of O 2p states and the conduction band is formed of Mg 3s states.

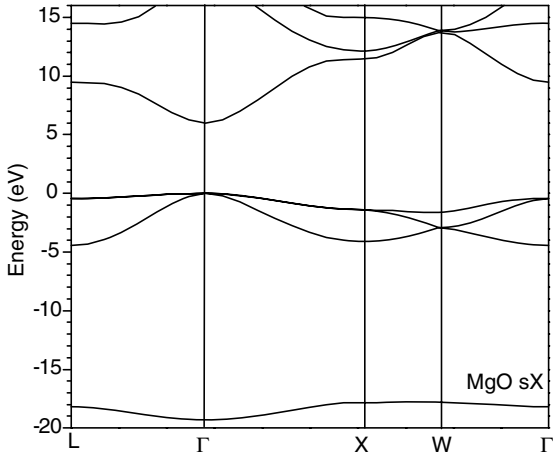

Figure 5.8 SX band structure of MgO in the rock salt structure.

5.3.4
Band Structures of SnO_2 and CdO

The three transparent conducting oxides ZnO, CdO and SnO_2 are good tests of band structure methods. ZnO has been treated already. CdO fails badly in GGA, where it is found to have a negative indirect band gap. In SX, the band gap is now positive, and 0.9 eV. This is close to the experimental value (Table 5.1). Note that CdO has an indirect gap from *L* to Γ, due to the effect of Cd d states on the upper valence band. Its conduction band is the standard free-electron like band, formed from Cd s states (Figure 5.9).

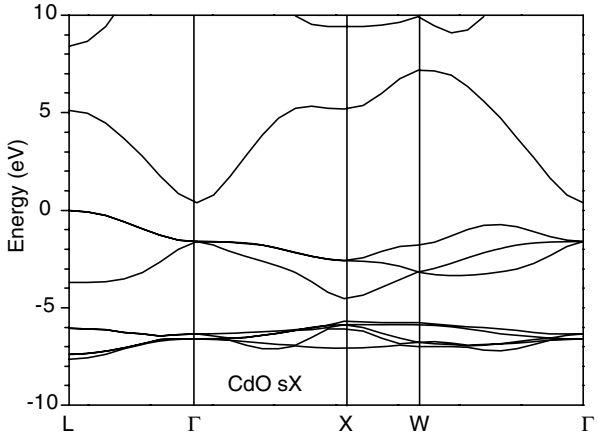

Figure 5.9 Calculated SX band structure of rock salt CdO. Note the real gap.

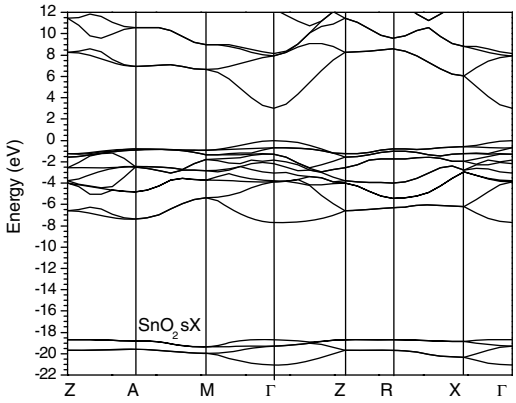

Figure 5.10 Calculated SX band structure of SnO_2 in the rutile structure.

SnO_2 has a simpler band structure, with a 3.6 eV direct-forbidden gap. However, in GGA the gap is typically only 0.9 eV. Figure 5.10 shows the calculated SX band structure, where the calculated gap is 3.6 eV, the experimental value. The band gaps between O 2p valence states and Sn s conduction band states.

5.3.5
Band Structure and Defects of HfO_2

We have carried out a SX calculations on various other oxides. HfO_2 is an important oxide in microelectronics as it is now used as the gate oxide in modern FETs. It is a closed shell transition metal oxide with a high dielectric constant. Figure 5.11 shows the band structure of cubic HfO_2 (fluorite structure) calculated by the SX functional [30]. The calculated band gap is slightly indirect and is 5.6 eV, which is

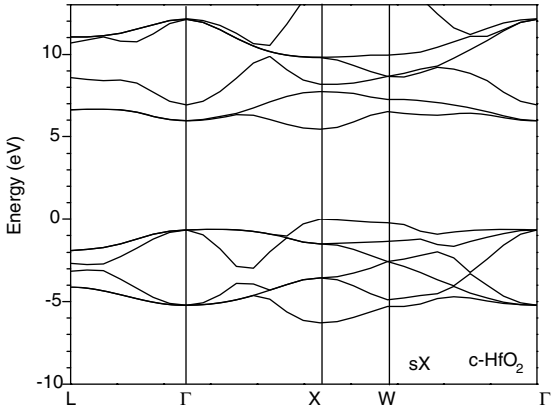

Figure 5.11 Band structure of cubic HfO_2 calculated by the SX method. The calculated band gap is 5.6 eV, compared to 5.8 eV experimentally.

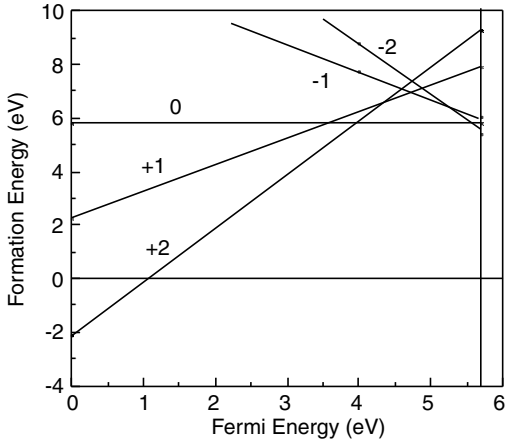

Figure 5.12 Defect formation energy versus Fermi energy for the oxygen vacancy in HfO_2, for an oxygen chemical potential of the O_2 molecule.

close to the experimental value of about 5.8 eV, whereas it is about 3.4–3.7 eV in LDA or GGA.

Defects are an important consideration in such oxides, as they lead to charge trapping, and an instability in the gate threshold voltage. The principle defect is now known to be the oxygen vacancy. From GGA calculations, it was unclear which defect was predominant, because GGA placed the vacancy levels either too low in the gap, or too high in the gap [75, 76], depending on which correction scheme was applied to the energy levels for the band gap error. SX played a critical role in resolving this question, as it was the first calculation of the oxygen vacancy levels which placed the energy levels correctly [30], and close to the experimental values observed by charge injection and optical absorption [77–81]. It was then realized that the oxygen vacancy was likely to be the main defect, as this is consistent with its behaviour in similar oxides such as ZrO_2.

Figure 5.12 shows the calculated SX formation energy of the oxygen vacancy versus the Fermi energy. The local structure was relaxed by SX. The lines represent the different charge states of the vacancy, and the transition states are where lines cross.

Figure 5.12 shows that the O vacancy is a negative U defect for both the -2 and $+1$ states. The calculated values are similar to those found by Gavartin *et al.* [82] and Broqvist and Pasquarello. [83] using the B3LYP and PBEh methods.

5.3.6
$BiFeO_3$

$BiFeO_3$ is the architypal multiferroic oxide, which shows both ferroelectric and antiferromagnetic properties. The interest arises from the possible electric field control of magnetic properties and vice versa. It is highly studied since it was made in thin film form on Si [84]. It has the R3c structure in its ferroelectric phase, which is

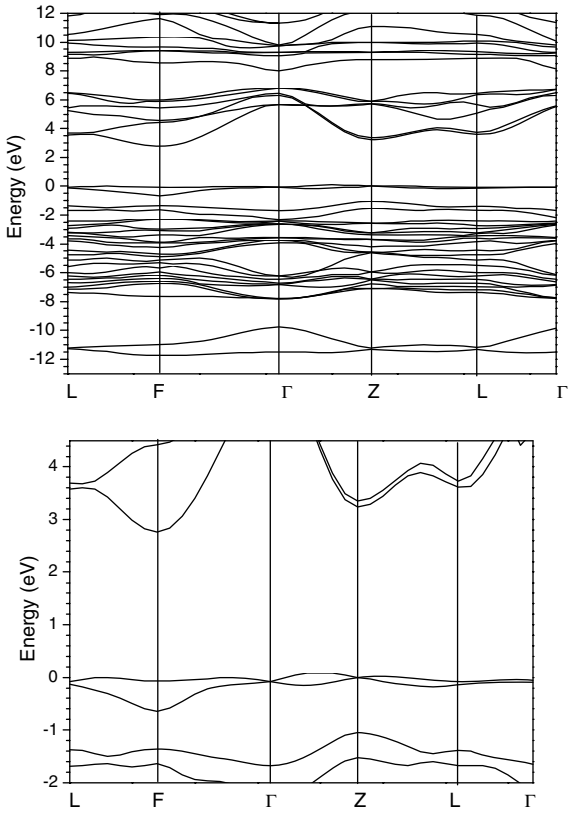

Figure 5.13 Calculated SX band structure of $BiFeO_3$ in the R3c structure, and close up of bands near the gap.

a small distortion of the cubic. It is a semiconductor whose band gap lies in the Fe 3d states of opposite spin (Figure 5.13).

There is no band gap in the LSDA method, even in the distorted structure. The simplest way to create a band gap is to use the LDA + U method, which does produce a band gap, as in the calculation of Neaton *et al.* [85]. However, the U parameter must be empirically chosen, which is unsatisfactory. We recently calculated the band structure of BFO by the SX method for the experimental structure, with no adjustable parameters [86, 87]. This gave a band gap of 2.7 eV, which was the first available value of the gap. It agrees with subsequent experimental evaluations [88, 89].

5.4 Summary

The SX method has been reviewed as a method to produce band structures of insulators and semiconductors with more accurate band gaps. SX behaves as a hybrid

density functional, which can be used for energy minimization. Some examples of the used of SX, particularly in oxides, are given.

Acknowledgements

The authors acknowledge valuable discussions with A. Zunger and S. Lany.

References

1 Sham, L.J. and Schluter, M. (1983) *Phys. Rev. Lett.,* **51**, 1888; Perdew, J.P. and Levy, M. (1983) *Phys. Rev. Lett.,* **51**, 1884; Godby, R.W., Schluter, M., and Sham, L.J. (1986) *Phys. Rev. Lett.,* **56**, 2415.
2 Gygi, F. and Baldereschi, A. (1989) *Phys. Rev. Lett.,* **62**, 2160.
3 Perdew, J.P. and Zunger, A. (1981) *Phys. Rev. B,* **23**, 5048.
4 Filippetti, A. and Spaldin, N.A. (2003) *Phys. Rev. B,* **67**, 125109.
5 Hedin, L. (1965) *Phys. Rev.,* **139A**, 796.
6 Hybertsen, M.S. and Louie, S.G. (1986) *Phys. Rev. B,* **34**, 5390.
7 Aryasetiawan, F. and Gunnarsson, O. (1998) *Rep. Prog. Phys.,* **51**, 2327.
8 Rohlfing, M., Kruger, P., and Pollmann, J. (1993) *Phys. Rev. B,* **48**, 17791.
9 Aulbur, W.G. Jonsson, L., and Wilkins, J. (2000) *Solid State Physics*, edited by Ehrenreich H. and Spaepen, F., Vol. 54 Academic Press, New York, p. 1.
10 van Schilfgaarde, M., Kotani, T., and Faleev, S. (2006) *Phys. Rev. Lett.,* **96**, 226402.
11 Anisimov, V.I., Zaanen, J., and Andersen, O.K. (1991) *Phys. Rev. B,* **44**, 943.
12 Anisimov, V.I., Aryasetiawan, F., and Lichtenstein, A.I. (1997) *J. Phys.: Condens. Matter,* **9**, 767.
13 Janotti, A. and van de Walle, C.G. (2006) *Phys. Rev. B,* **74**, 045202.
14 Becke, A.D. (1993) *J. Chem. Phys.,* **98**, 1372.
15 Perdew, J.P., Ernzerhof, M., and Burke, K. (1996) *J. Chem. Phys.,* **105**, 9982.
16 Muscat, J., Wander, A., and Harrison, N.M. (2001) *Chem. Phys. Lett.,* **342**, 397.
17 Paier, J., Hirschl, R., Marsman, M., and Kresse, G. (2005) *J. Chem. Phys.,* **122**, 234102.
18 Heyd, J. Scuseria, G.E., and Ernzerhof, X.X. (2003) *J. Chem. Phys.,* **118**, 8207.
19 Heyd, J. and Scuseria, G.E. (2004) *J. Chem. Phys.,* **120**, 7274.
20 Heyd, J., Peralta, J.E., Scuseria, E., and Martin, R.L. (2005) *J. Chem. Phys.,* **123**, 174101.
21 Krukau, A.V., Vydrov, O.A., Izmaylov, A.F., and Scuseria, G.E. (2006) *J. Chem. Phys.,* **125**, 224106.
22 Paier, J., Marsman, M., Hummer, K., Kresse, G., Gerber, I.C., and Angyan, J.G. (2006) *J. Chem. Phys.,* **124**, 154709.
23 Bylander, D.M. and Kleinman, L. (1990) *Phys. Rev. B,* **41**, 7868.
24 Seidl, A., Gorling, A., Vogl, P., Majewski, J.A., and Levy, M. (1996) *Phys. Rev. B,* **53**, 3764.
25 Geller, C.B., Wolf, W., Picozzi, S., Continenza, A., Freeman, A.J., and Wimmer, E. (2001) *Appl. Phys. Lett.,* **79**, 368.
26 Asahi, R., Wang, A., Babcock, J.R., Edelman, N.L., Metz, A.W., Lane, M.A., Dravid, V.P., Kannewurf, C.R., Freeman, A.J., and Marks, T.J. (2002) *Thin Solid Films,* **411**, 101.
27 Segall, M.D., Lindan, P.J.D., Probert, M.J., Pickard, C.J., Hasnip, P.J., Clark, S.J., and Payne, M.C. (2002) *J. Phys.: Condens. Matter,* **14**, 2717.
28 Rappe, A.M., Rabe, K.M., and Joannopoulos, J.D. (1996) *Phys. Rev. B,* **41**, 1227.
29 Gibson, M.C., Brand, S., and Clark, S.J. (2006) *Phys. Rev. B,* **73**, 125120.
30 Xiong, K., Robertson, J., Gibson, M.C., and Clark, S.J. (2005) *Appl. Phys. Lett.,* **87**, 183505.
31 Robertson, J., Xiong, K., and Clark, S.J. (2006) *Phys. Status Solidi B,* **243**, 2054; (2006) *Phys. Status Solidi B,* **243**, 2071.

32 Clark, S.J. and Robertson, J. (2007) *Appl. Phys. Lett.,* **90**, 132903; (2009) *Appl. Phys. Lett.,* **94**, 022902. Liu, D. Clark, S.J., and Robertson, J. (2010) *Appl. Phys. Lett.,* **96**, 032905.

33 Vanheusden, K., Warren, W.L., Seager, C.H., Taliant, D.R., Voigt, J.A., and Gnade, B.E. (1996) *J. Appl. Phys.,* **79**, 7983.

34 Ozgur, U. *et al.,* (2005) *J. Appl. Phys.,* **98**, 041301.

35 Look, D.C., Chaflin, B., Allvov, Y.I., and Park, S.J. (2004) *Phys. Status Solidi A,* **201**, 2203.

36 Look, D.C. and Chaflin, B. (2004) *Phys. Status Solidi B,* **241**, 624.

37 Tsukazaki, A. *et al.* (2005) *Nature Mater,* **4**, 42.

38 Tsukazaki, A., Ohtomo, A., Kita, T., Ohno, Y., Ohno, H., and Kawasaki, M. (2007) *Science,* **315**, 1388.

39 Pearton, S.J., Heo, W.H., Ivill, M., Norton, D.P., and Steiner, T. (2004) *J. Phys.: Condens. Matter,* **19**, R59.

40 Zhang, S.B., Wei, S.H., and Zunger, A. (2001) *Phys. Rev. B,* **63**, 075205. Zhang, S.B., Wei, S.H., and Zunger, A. (1998) *J. Appl. Phys.,* **83**, 3192.

41 Lyons, J.L., Janotti, A., and van de Walle, C.G. (2009) *Appl. Phys. Lett.,* **95**, 252105.

42 Chelikowsky, J.R. (1977) *Solid State Commun.,* **22**, 351.

43 Schroer, P., Kruger, P., and Pollmann, J. (1993) *Phys. Rev. B,* **47**, 6971.

44 Vogel, D., Kruger, P., and Pollmann, J. (1995) *Phys. Rev. B,* **52**, R14316.

45 Usuda, J.M., Hamada, N., Kotani, T., and van Schilfgaarde, M. (2002) *Phys. Rev. B,* **66**, 125101.

46 Fuchs, F., Furthmüller, J., Bechstedt, F., Shishkin, M., and Kresse, G. (2007) *Phys. Rev. B,* **76**, 115109.

47 Preston, A.H.R., Ruck, B.J., Piper, L.F.J., DeMasi, A., Smith, K.E., Schleife, A., Fuchs, F., Bechstedt, F., Chai, J., and Durbin, S.M. (2008) *Phys. Rev. B,* **78**, 155114.

48 Uddin, J. and Scuseria, G.E. (2006) *Phys. Rev. B,* **74**, 245115.

49 Kohan, A.F., Ceder, G. Morgan, D., and van de Walle, C.G. (2000) *Phys. Rev. B,* **61**, 15019.

50 Janotti, A. and van de Walle, C.G. (2005) *Appl. Phys. Lett.,* **87**, 122102.

51 Janotti, A. and Van de Walle, C.G. (2007) *Phys. Rev. B,* **76**, 165202.

52 Oba, F., Togo, A., Tanaka, I., Paier, J., and Kresse, G. (2008) *Phys. Rev. B,* **77**, 245202.

53 Erhart, P., Albe, K., and Klein, A. (2006) *Phys. Rev. B,* **73**, 205203.

54 Patterson, C.H. (2006) *Phys. Rev. B,* **74**, 144432.

55 Paudel, T.R. and Lambretch, W.R.L. (2008) *Phys. Rev. B,* **77**, 205202.

56 Agoston, P., Albe, K., Nieminen, R.M., and Puska, M.J. (2009) *Phys. Rev. Lett.,* **103**, 245501.

57 Lany, S. and Zunger, Av. (2005) *Phys. Rev. B,* **72**, 035215.

58 Lany, S. and Zunger, A. (2007) *Phys. Rev. Lett.,* **98**, 045501.

59 Lany, S. and Zunger, A. (2008) *Phys. Rev. B,* **78**, 235104.

60 Lany, S. and Zunger, A. (2010) *Phys. Rev. B,* **81**, 113201.

61 Clark, S.J., Robertson, J., Lany, S., and Zunger, A. (2010) *Phys. Rev. B,* **81**, 115311.

62 Van de Walle, C.G. (2000) *Phys. Rev. Lett.,* **85**, 1012.

63 Lee, E.C., Kim, Y.S., Jin, Y.G., and Chang, K.J. (2001) *Phys. Rev. B,* **64**, 085120.

64 Girard, R.T., Tjernberg, O., Chiaia, G., Soderholm, S., Jarlsson, U.O., Wigren, C., Nylen, H., and Lindau, I. (1997) *Surf. Sci.,* **373**, 409.

65 Ozawa, K., Sawada, K., Shirotori, Y., and Edamoto, K. (2005) *J. Phys.: Condens. Matter,* **17**, 1271.

66 Probert, M.I.J. and Payne, M.C. (2003) *Phys. Rev. B,* **67**, 075204.

67 Look, D.C., Hemsky, J.W., and Sizelove, J.R. (1999) *Phys. Rev. Lett.,* **82**, 2552.

68 Hagemark, K.I. and Toren, P.E. (1975) *J. Electrochem. Soc.,* **122**, 992. Tuomisto, F. *et al.,* (2003) *Phys. Rev. Lett.,* **91**, 205502.

69 Selin, F.A., Weber, M.H., Solodovnikov, D., and Lynn, K.G. (2007) *Phys. Rev. Lett.,* **99**, 085502.

70 Vlasenko, L.S. and Watkins, G.D. (2005) *Phys. Rev. B,* **71**, 125210.

71 Pacchioni, G., Frigoli, F., Ricci, D., and Weil, J.A. (2000) *Phys. Rev. B,* **63**, 054102. d'Avezac, M., Calandra, M., and Mauri, F. (2005) *Phys. Rev. B,* **71**, 205210.

72 Lany, S. and Zunger, A. (2009) *Phys. Rev. B,* **80**, 085202.

73 Galland, D. and Herve, A. (1970) *Phys. Lett. A,* **33**, 1.

74 Vlasenko, L.S. and Watkins, G.D. (2005) *Phys. Rev. B,* **72**, 035203.

75 Foster, A.S., Sulimov, V.B., Gejo, F.L., Shluger, A.L., and Nieminen, R.N. (2001) *Phys. Rev. B,* **64**, 224108.

76 Shen, C., Li, M.F., Yu, H.Y., Wang, X.P., Yeo, Y.C., Chan, D.S.H.,, and Kwong, D.L. (2005) *Appl. Phys. Lett.,* **86**, 093510.

77 Kerber, A., Cartier, E., Pantisano, L., Degraeve, R., Kauerauf, T., Kim, Y., Groeseneken, G., Maes, H.E., and Schwalke, U. (2003) *IEEE Electron Device Lett.,* **24**, 87.

78 Cartier, E. *et al.* (2006) Tech Digest IEDM.

79 Takeuchi, H., Ha, D., and King, T.J. (2004) *J. Vac. Sci. Technol. A,* **22**, 1337.

80 Nguyen, N.V., Davydov, A.V., Chandler-Horowitz, D., and Frank, M.M.M. (2005) *Appl. Phys. Lett.,* **87**, 192903.

81 Walsh, S., Fang, L., Schaeffer, J.K., Weisbrod, E., and Brillson, L.J. (2007) *Appl. Phys. Lett.,* **90**, 052901.

82 Gavartin, J.L., Ramos, D.M., Shluger, A.L., Bersuker, G., and Lee, B.H. (2006) *Appl. Phys. Lett.,* **89**, 082908.

83 Broqvist, P. and Pasquarello, A. (2006) *Appl. Phys. Lett.,* **89**, 262904.

84 Wang, J., Neaton, J.B., Zheng, H., Nagarajan, V., Ogale, S.B., Liu, B., Viehland, D., Vaithyanathan, V., Schlom, D.G., Waghare, U.V., Spaldin, N.A., Rabe, K.M., Wuttig, M., and Ramesh, R. (2003) *Science,* **299**, 1719.

85 Neaton, J.B., Ederer, C., Waghmare, U.V., Spaldin, N.A., and Rabe, K.M. (2005) *Phys. Rev. B,* **71**, 014113.

86 Clark, S.J., and Robertson, J. (2007) *Appl. Phys. Lett.,* **90**, 132903.

87 Palai, R., Katiyar, R.S., Schmid, H., Tissot, P., Clark, S.J., Robertson, Jv., Redfern, S.A.T., Catalan, G., and Scott, J.F. (2008) *Phys. Rev. B,* **77**, 014110.

88 Ihlefeld, J.F., Podraza, N.J., Liu, Z.K., Rai, R.C., Ramesh, R., and Schlom, D.G. (2008) *Appl. Phys. Lett.,* **92**, 142908.

89 Hauser, A.J., Zhang, J., Meier, L., Ricciardo, R.A., Woodward, P.M., Gustafson, T.L., Brillson, L.J., and Yang, F.Y. (2008) *Appl. Phys. Lett.,* **92**, 222901.